



Research Article

Investigating the growth of AlGa_N/AlN heterostructure by modulating the substrate temperature of AlN buffer layer



Neha Aggarwal¹ · Shibin Krishna² · Lalit Goswami¹ · Shubhendra Kumar Jain^{1,3,6} · Akhilesh Pandey⁴ · Abhiram Gundimeda⁵ · Pargam Vashishtha^{1,6} · Jasveer Singh¹ · Sandeep Singh¹ · Govind Gupta^{1,6} 

Received: 12 November 2020 / Accepted: 25 January 2021
© The Author(s) 2021 

Abstract

We have investigated the impact of AlN buffer layer growth parameters for developing highly single crystalline AlGa_N films. The low mobility of Al adatoms and high temperature for compound formation are amongst the major causes that affects the growth quality of AlGa_N films. Thus, proper optimization need to be carried out for achieving high quality AlGa_N due to an augmented tendency of defect generation compared to Ga_N films. Thus, growth conditions need to be amended to maximize the incorporation ability of adatoms and minimize defect density. So, this study elaborates the growth optimization of AlGa_N/AlN/Si (111) heterostructure with varied AlN buffer growth temperature (760 to 800 °C). It was observed that the remnant Al in low temperature growth of AlN buffer layer resist the growth quality of AlGa_N epitaxial films. A highly single crystalline AlGa_N film with comparatively lowest rocking curve FWHM value (~0.61°) and smooth surface morphology with least surface defect states was witnessed when AlN buffer was grown at 780 °C. From the Vegard's law, the photoluminescence analysis unveils Aluminium composition of 31.5% with significantly reduced defect band/NBE band ratio to 0.3. The study demonstrates good crystalline quality AlGa_N film growth with Aluminium content variation between ~30–39% in AlGa_N/AlN heterostructure on Si(111) substrate leading to a bandgap range which is suitable for next-generation solar-blind photodetection applications.

Keywords AlGa_N film · Epitaxial growth · PAMBE · Crystalline quality · Al incorporation

1 Introduction

A ternary alloy of III-Nitride material system i.e. Al_xGa_{1-x}N has huge number of potential applications in high power and radiation-resistance electronics such as flame and heat detectors, missile plume detection and safe inter-satellite communications, UV calibration and monitoring devices for medical and biological sensors, etc. [1–3]. In the past few

years, these applications were fulfilled by photomultiplier tubes, SiC and Si based detectors [4]. Sooner the photomultiplier tubes are found to be inefficient due to bulky instrumentation while, Si, having a narrow bandgap of 1.1 eV, demands optical filters to function as a UV detector which again makes the system massive and costly. However, bandgap of Al_xGa_{1-x}N can be tuned between 3.4 eV (at 0% Al) and 6.2 eV (at 100% Al) thus; it offers a great advantage over Si by

Supplementary information The online version of this article (<https://doi.org/10.1007/s42452-021-04274-4>) contains supplementary material, which is available to authorized users.

✉ Govind Gupta, govindnpl@gmail.com | ¹CSIR-National Physical Laboratory (NPL), Dr. K. S. Krishnan Marg, New Delhi 110012, India. ²Advanced Semiconductor Laboratory, King Abdullah University of Science and Technology, Thuwal 23955, Saudi Arabia. ³Functional Materials and Microsystems Research Group and the Micro Nano Research Facility, RMIT University, Melbourne, VIC 3000, Australia. ⁴Solid State Physics Laboratory, Defence Research and Development Organization, Timarpur, Delhi 110054, India. ⁵Department of Materials Science and Metallurgy, University of Cambridge, Cambridge CB3 0FS, UK. ⁶Academy of Scientific and Innovative Research, CSIR-HRDC Campus, Ghaziabad, Uttar Pradesh 201002, India.



SN Applied Sciences

(2021) 3:291

| <https://doi.org/10.1007/s42452-021-04274-4>

Published online: 08 February 2021

SN Applied Sciences
A **SPRINGER NATURE** journal

eliminating the need of optical filters [5]. Besides the robustness of $\text{Al}_x\text{Ga}_{1-x}\text{N}$ material, it also provides the potential to yield stable device operation even in harsh environments [6, 7]. On the other hand, SiC, having a bandgap of ~ 3.0 eV is similar in robustness to nitrides, still does not have the potential to tune the bandgap via alloying and thus, they require expensive filters for UV applications [5, 8]. Since, an ideal optoelectronic device necessitates deeper understanding about various factors affecting optical and electrical transport properties of the thin films. The major challenge that hinders the development of highly efficient AlGaN/AlN heterostructure based devices is the high quality growth on suitable substrate as this will directly impact the structural and optical properties which ultimately alter the current transport behavior in the device. Usually, high quality AlGaN has been grown on sapphire substrates or GaN templates for better growth quality [9–11] but soon researchers started growing AlGaN on Si substrates for better integration with existing established device fabrication technology [12–15]. Here, Si substrate is utilized because it is easily available at low cost & provides integration with the well-established Si growth technology that ensures high quality device fabrication as well. However, the direct growth of AlGaN on Si substrate may lead to high amount of defects and cracks due to lattice-mismatch and thermal expansion coefficient mismatch between the substrate and the epitaxial film [5]. Consequently, these defects states instigate degradations in structural, morphological and optical properties. Thus, introduction of a buffer layer is extremely necessary as it plays a key role in improving the crystalline quality and reducing the defect states in epitaxial AlGaN films grown by plasma-assisted molecular beam epitaxy (PAMBE) system [16, 17]. However, most of the studies report AlGaN growth on Si using GaN buffer layer and only few reports elaborate the growth on Si using AlN buffer [3, 18]. Although, the effect of AlN buffer layer has been vastly studied [19, 20] on the properties of GaN films still its role on AlGaN/AlN heterostructure grown on Si (111) has not yet explored much in detail. Hence, this work explicates the influence of AlN buffer layer on the crystalline quality and defect density of epitaxially grown AlGaN films by PAMBE. The present study also correlates the role of different AlN buffer growth temperatures with the structural, morphological and optical properties of AlGaN films including compositional variations that result in bandgap variation as well.

2 Materials and methods

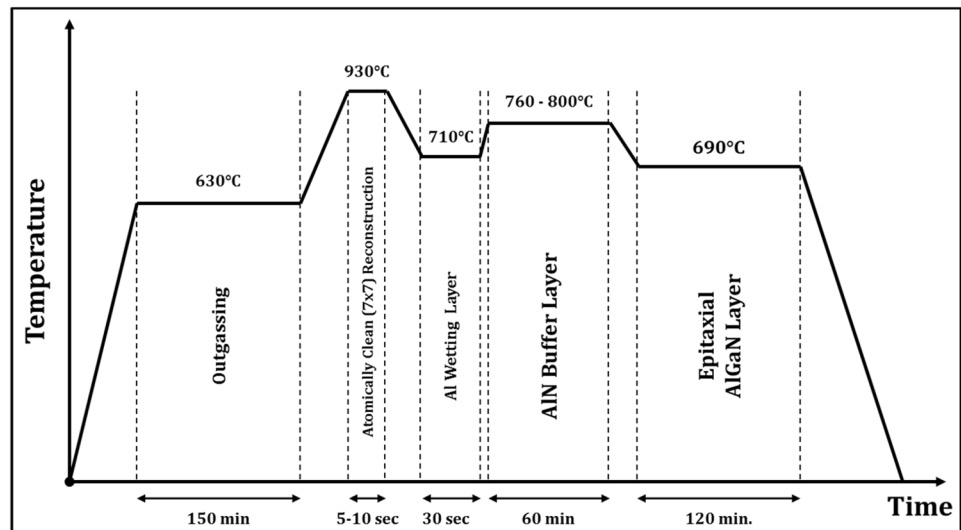
The AlGaN/AlN heterostructures were grown on p-Si (111) substrate (325 ± 25 μm thick, boron doped (p-type) with resistivity of 5–15 $\Omega\text{-cm}$) by PAMBE system. The (111) orientation of Si substrate is utilized in this study

because the growth of wurtzite hexagonal AlN (002) is more preferred on Si (111) over other orientations of silicon substrate which leads to good quality nitride heterostructure [21]. The silicon substrates were chemically pre-cleaned by using the standard RCA procedure before loading into the load-lock chamber followed by out-gassing in the buffer chamber at 630 $^\circ\text{C}$.

Prior to growth, the Si substrates were flashed at high temperature in the growth chamber to achieve atomically clean 7×7 reconstructed surfaces. Initially, ~ 480 nm thick AlN buffer layer is grown on Si substrate since, the introduction of AlN buffer layer may lead towards crack free growth. Thus, a number of samples have been grown with varied growth parameters of AlN and some of them are discussed in this study to avail better understanding about role of buffer layer growth conditions on the AlGaN epitaxial layer. A growth-time vs temperature diagram representing each step involved in the growth process is shown in Fig. 1. The diagram illustrates that the growth procedure starting from the outgassing of substrate to obtaining an epitaxial AlGaN heterostructure takes nearly 330 min. to complete. Here, three samples are being discussed which are grown with different AlN substrate temperatures varied between 760 to 800 $^\circ\text{C}$ and labelled according to buffer growth temperature i.e., S-760, S-780 and S-800. Apart from the substrate temperature of AlN, rest all other growth parameters are kept constant in complete growth process of all the samples. Then, ~ 1.5 μm thick AlGaN has been grown with a constant pre-optimized parameters on the AlN buffer with varied growth temperature. The substrate temperature, BEP of Ga and Al, N_2 flux as well as RF power and growth time during AlGaN growth was set to 690 $^\circ\text{C}$, 2×10^{-6} Torr, 2×10^{-7} Torr, 3 sccm, 400 W and 120 min, respectively. Therefore, the effects of AlN buffer layer were elaborated via various structural, morphological and optical properties of PAMBE grown epitaxial AlGaN film.

The structural quality of the grown films was gauged by using high resolution X-ray diffraction (HRXRD, Panalytical X'Pert PRO MRD System), and the surface morphology was probed by atomic force microscopy (AFM, Multimode-V Veeco) and FESEM (ZEISS AURIGA). The optical properties, bandgap evaluations and stress variations have been reckoned by using photoluminescence (PL) and Raman spectroscopy (RS), respectively. PL measurements were carried out using FLS980 D2D2 (Edinburg) system equipped with a He – Cd laser operating at 325 nm as an excitation source. Room temperature (RT) micro-Raman measurements were performed using a triple Raman spectrometer in backscattering configuration with an excitation source of argon ion laser (Ar+) having an operating wavelength of 514 nm.

Fig. 1 The growth-time–temperature diagram representing complete timeline of developing epitaxial AlGa_n on Si (111) substrate



3 Results and discussions

A systematic study of the hetero-epitaxial growth of AlGa_n/AlN on Si (111) via PAMBE has been illustrated by using a number of samples grown with varied buffer layer growth parameters. Depending upon the buffer layer growth conditions, physical as well as optical properties of the epitaxial AlGa_n film may differ. Several properties of the grown heterostructure is analyzed deeply and discussed as follows.

3.1 Structural properties

A schematic diagram showed in Fig. 2a represents the PAMBE grown heterostructure where initially AlN film is grown on atomically cleaned Si (111) surface which act as buffer layer for the epitaxial growth of AlGa_n film. The AlGa_n films grown on the three distinct AlN buffer layers has been characterized by HRXRD measurements to examine the quality of grown AlGa_n/AlN/Si (111) heterostructure. Figure 2b illustrates the HRXRD 2θ-omega scan of S-760 sample where the highly intense and sharp peaks at 35.04° and 36.08° explicates the growth of single crystalline AlGa_n and AlN films, respectively. Moreover, the presence of first and second order X-ray diffractions of AlGa_n in the 2θ-omega scan endorses that single crystalline AlGa_n film has been successfully grown epitaxially on the Si substrate. Besides, the sharp peaks at 28.4° and 58.8° have been derived from the first and second order diffractions of Si (111). An additional peak at ~31.8° has been observed in Fig. 2b and Fig. 2c which is found to be associated with the (002) orientation of α-Si₃N₄ that might have formed while exposing the substrate to active N species for AlN growth [22].

Further, HRXRD analysis of S-780 sample (Fig. 2c) indicates that high temperature buffer can yield improved crystalline quality of AlGa_n by observing very sharp peaks with reduced FWHM value. It has been clearly witnessed that the intensity ratio of AlGa_n/AlN in S-760 (9.75) is more compared to S-780 sample (3.48). This can be attributed to a slight remnant Al present in low temperature (760 °C) grown AlN as confirmed from a small peak at 38.1° in 2θ-omega scan of S-760 (in Fig. 2 (b) which was absent in the sample S-780 where AlN is grown at a slightly higher temperature (780 °C) leading to improved AlN quality as well as AlGa_n epitaxial quality. This signifies that the remnant Al (in S-760) must have resisted the growth of AlGa_n film thereby, affecting its growth rate and quality. However, upon further increasing the AlN buffer growth temperature to 800 °C in S-800 sample, HRXRD analysis shown in Fig. 2d) reveals that such high temperature buffer can lead to a reduction in peak intensity of AlGa_n as well as AlN as observed from the plot peaks in S-800 with reduced intensity compared to S-780. This analysis reveals that higher growth temperature results in lower growth rate of AlN buffer which slows down the growth rate of AlGa_n epitaxial film as well. Thus, the sharp and intense peaks signify highly single crystalline nature of AlN and AlGa_n films in each grown heterostructure optimized to a best crystallinity and highest intensity in S-780 sample.

For better understanding, the average grain size for AlN and AlGa_n layers has been evaluated by using the Scherrer formula: [20, 23]

$$t = K \cdot \lambda / \beta \cos \theta \quad (1)$$

Here, 't' is the average grain size, 'K' is a proportionality constant (assumed value near to unity), 'λ' is the wavelength of the incident beam (0.15406 nm), 'β' is the

Fig. 2 **a** A schematic diagram of heterostructure grown via PAMBE; HRXRD 2θ —omega scans of grown epitaxial structure in **b** S-760; **c** S-780 and **d** S-800

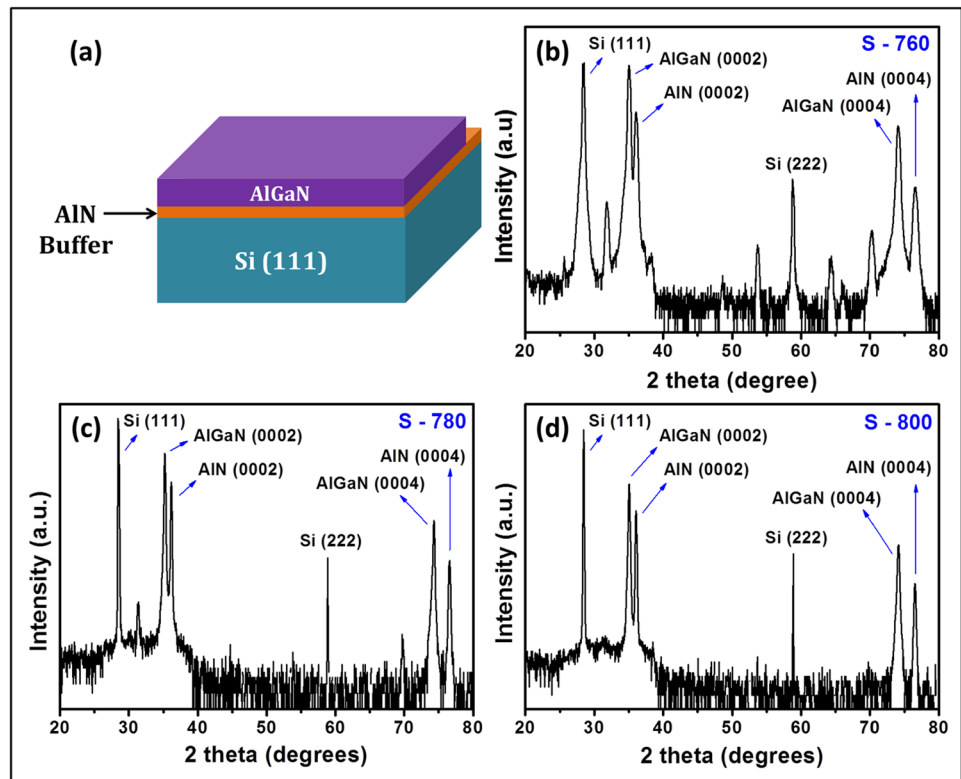


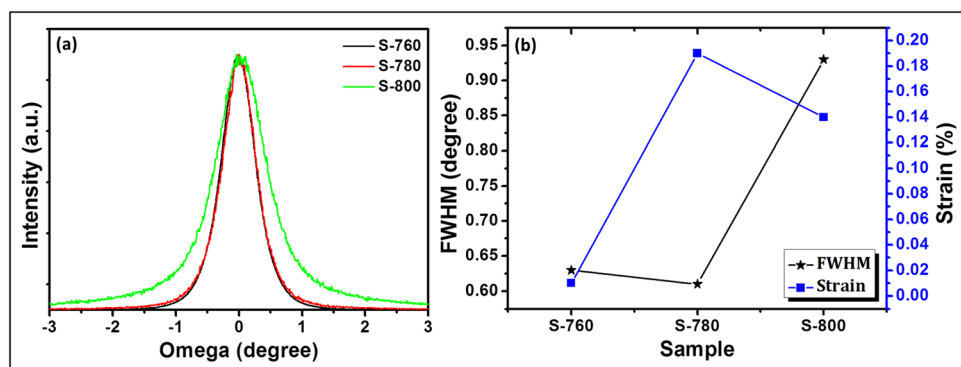
Table 1 The evaluated average grain sizes of AlN and AlGaIn grown with varied buffer layer temperatures

Material	Average grain size (nm)		
	S-760	S-780	S-800
AlN	24.75	49.97	44.82
AlGaIn	26.72	52.05	49.02

FWHM of the AlN and AlGaIn peak from 2θ —omega scan of HRXRD pattern along (0002) plane of diffraction (in radians), and ‘ θ ’ is the diffraction angle of the AlN (0002) and AlGaIn (002) peaks. The grain sizes obtained by the Scherrer formula are tabulated in Table 1.

It was clearly observed from Table 1 that the average grain size is largest for the AlN and AlGaIn grown in S-780 sample which is suggesting that the buffer growth temperature of 780 °C is providing adequate amount of surface energy to the ad-atoms arriving at the surface for growing the desired nitride heterostructure. Next, to quantify the crystalline quality of grown films, the X-ray rocking curves (XRCs) has been utilized which are plotted in Fig. 3a where the evaluated FWHM value is 0.63°, 0.61° arcsec and 0.93° along in-plane (002) diffraction from samples S-760, S-780 and S-800, respectively (Fig. 3b). The FWHM values are directly related to the dislocation density existing in the grown layer which will lately govern the performance of an optoelectronic

Fig. 3 **a** The comparative XRC plots of AlGaIn along (0002) plane of diffraction; **b** The trends revealing variation in FWHM from XRCs and strain evaluated for epitaxial AlGaIn films with changing buffer growth temperatures

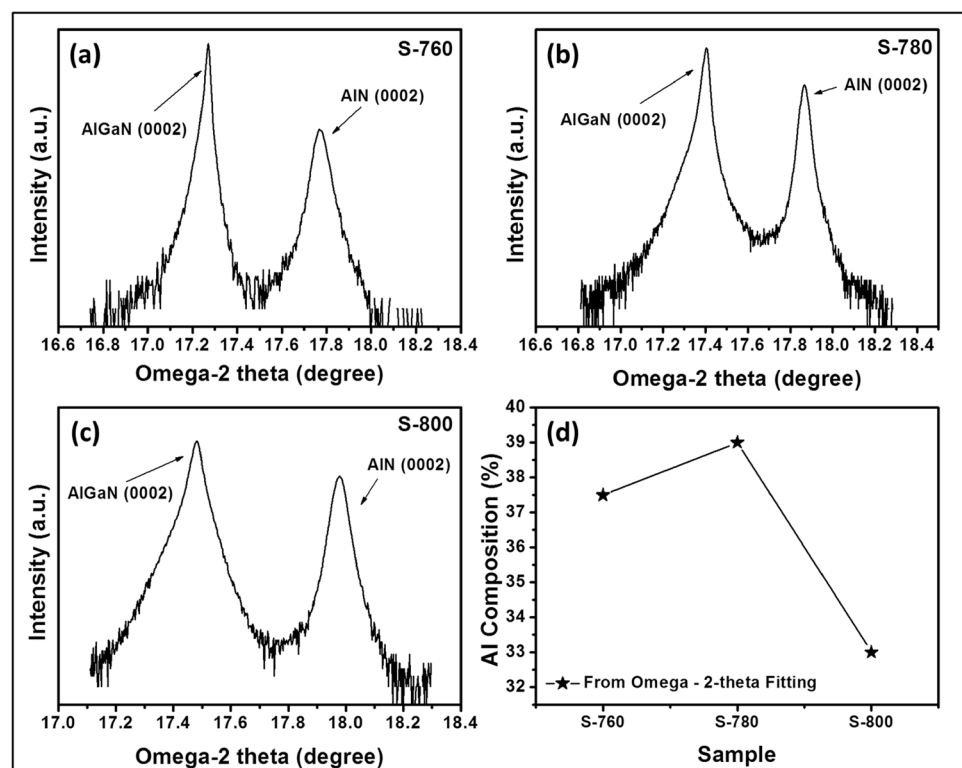


device to be developed using them [24]. It is interesting to notice that the FWHM value of S-780 sample is lower than other two samples grown with varied buffer via PAMBE and some previous reports of AlGa_N growth on Si (111) [25]. The lower value of the FWHM in sample S-780 exemplifies low mosaicity of the grown film and can be correlated to better formation of AlN which resulted in enhanced crystalline quality of the epitaxial AlGa_N film. The FWHM and strain variation is represented in Fig. 3b where the strain values have been evaluated by using the peak positions of 2 θ -omega scans in Bragg's law [26].

Here, the strain free values were assumed to be the lattice constants corresponding to the Al compositions evaluated from omega-2 θ scans which will be discussed next in this section. Upon quantifying, the strain values are found to be 0.01 GPa, 0.19 GPa and 0.14 GPa for S-760, S-780 and S-800, respectively. The higher strain value in S-780 implies strained film which may or may not lead to cracks that can further be affirmed by observing the morphological properties of the grown AlGa_N films. The topographical study has been discussed in next section for gaining deeper understanding into it. Before that, the omega-2 theta scan has been carried out for the determination of Al composition in PAMBE grown AlGa_N films. Figure 4a–c shows the omega-2 theta scan HRXRD spectra along the symmetric (0002) plane of diffraction from the AlGa_N and AlN films.

The fitting of these spectra (not shown here) revealed the Al composition of 37.5%, 39% and 33% in sample S-760, S-780 and S-800, respectively. The evaluated Al composition variation is plotted against sample in Fig. 4d. It was noticed that the Al composition is highest in sample S-780 due to optimized buffer conditions which lead to better AlN quality and thereby, enhanced AlGa_N crystallinity along with higher Al incorporation. The physical mechanism and surface kinetics defined by the buffer growth temperature towards increasing the Al incorporation in S-780 sample is explained as follows. At lower growth temperature (760 °C) of AlN buffer layer, the HRXRD analysis of 2 θ -omega scan shows a small peak at ~38.20° which is associated with the presence of excess metallic Al at the interface. [3] This is due to inadequate surface energy at lower temperature which limits the conversion of all the arriving Al ad-atoms into AlN compound, resulting in remnant Al at the interface. So, when the surface is exposed to Al, Ga ad-atoms and N active species for AlGa_N growth, it was observed that initially the excess Al utilizes the nitrogen to form AlN restricting the formation of AlGa_N and later on, the growth of AlGa_N was pursued leading to lower Al incorporation in the AlGa_N layer. Secondly, at the higher temperature of 800 °C, nitrogen rich condition leads to III-group vacancies. Upon exposing the surface with Al, Ga and N for AlGa_N growth, these vacancies are initially filled by III-group elements which should be

Fig. 4 HRXRD omega-2theta scans of epitaxial AlGa_N films grown in **a** S-760; **b** S-780 and **c** S-800 samples; **d** Al compositions evaluated by fitting of omega-2 θ scans



followed by the AlGa_N growth. This leads to lower incorporation of Al in AlGa_N layer since the growth time and Al flux is kept constant in all the three samples. Finally, in the stoichiometric conditions of sample S-780, there was no remnant Al after AlN deposition and also no III-group vacancies due to optimum growth temperature of AlN buffer layer. This leads to smooth and quick start for the growth of AlGa_N as soon as the surface was exposed to the Al, Ga and N adatoms. This must result in highest incorporation of Al in the AlGa_N grown in S-780. Next, the influence of buffer quality on surface morphology of AlGa_N has been examined by analyzing the FESEM and AFM micrographs shown in Fig. 5.

3.2 Morphological properties

Figure 5 displays the topographical features of the top AlGa_N surface in all the grown AlGa_N/AlN heterostructures. The influence of buffer growth temperature has been clearly witnessed by the variations in surface morphology of AlGa_N. The FESEM, AFM and depth profiles are shown in Fig. 5 (a,d,g), (b,e,h) and (c,f,i) for the AlGa_N surface in samples S-760, S-780 and S-800, respectively. It can be observed from the FESEM image of S-760 (Fig. 5a) that the surface is quite smooth with the presence of few nano-islands while, a highly smooth surface with almost coalesced epitaxial film is witnessed in the FESEM image of S-780 (Fig. 5d) and the nano-islands observed in S-760 has also been reduced effectively. However, when the AlN growth temperature increased to 800 °C in S-800,

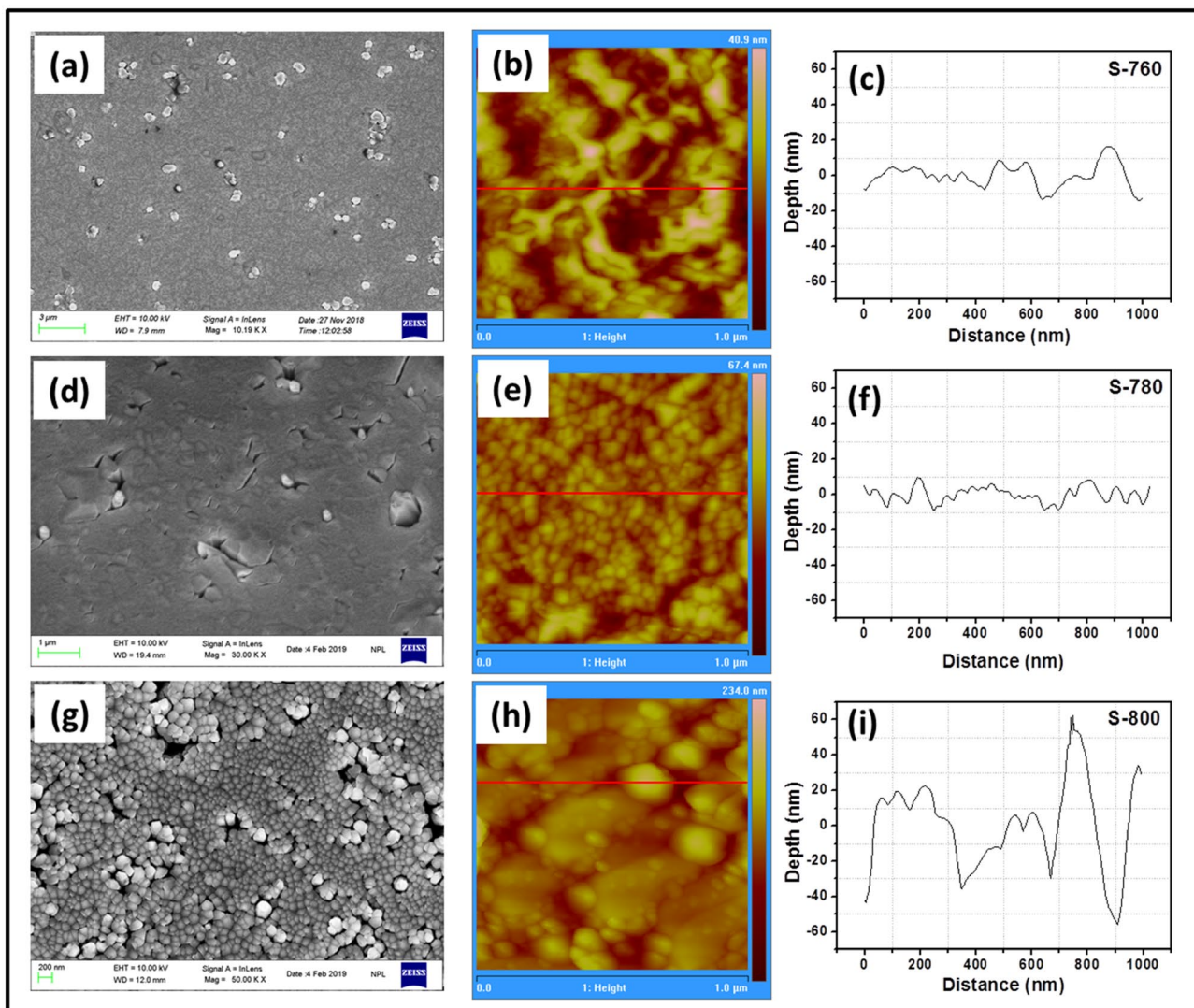


Fig. 5 The topographical analysis using (a,d,g) FESEM; (b,e,h) AFM and (c,f,i) Depth profiling (via AFM where the area is marked by red line) for samples S-760, S-780 and S-800, respectively

the surface becomes quite rough with huge nano-sized islands agglomerated into an epitaxial film as shown in Fig. 5g. Therefore, it can be concluded that the film grown in sample S-780 has smoother surface morphology along with less surface defects than the films grown in samples S-760 and S-800.

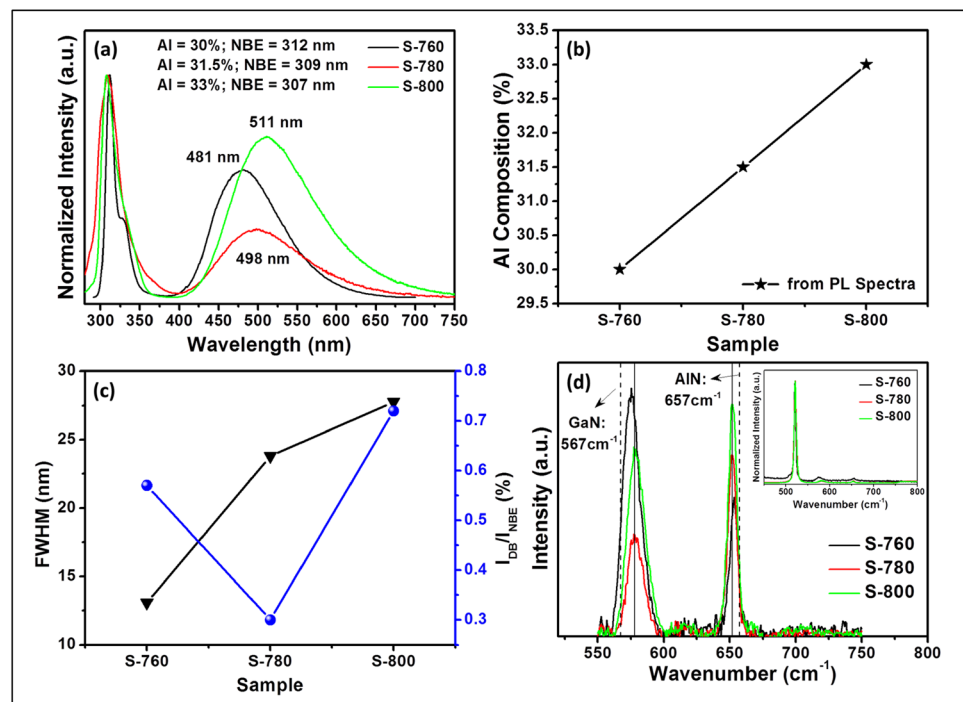
Furthermore, to avail better understanding of morphological properties, the surface was probed by AFM which will divulge the surface morphology along with surface roughness and its depth profile. The AFM image of AlGaIn film grown in S-760 (Fig. 5b) shows slightly smooth surface morphology ($r.m.s.$ roughness, $R_{r.m.s.} = 6.44$ nm) covered with small troughs which were assumed to be appeared due to the nitrogen vacancies in epitaxial AlN buffer layer that was grown in Al-rich conditions [27]. As the buffer growth temperature increases to 780 °C (Fig. 5e), the active nitrogen species is expected to be entirely consumed by the impinging Al flux due to sufficiently available thermal energy on the substrate and thereby, growing high quality AlN layer effectively improved the surface morphology of AlGaIn layer to a greater extent [28]. An effective reduction in surface roughness has been witnessed with the $R_{r.m.s.}$ value of 5.62 nm which may lead to better carrier transport if utilized for device fabrication. This has been correlated with the high strain value evaluated from HRXRD that mutually explicate highly smooth and slightly strained film surface by restricting the crack formation which sometimes appear due to strain relaxation. Recently, Singh et al. reported that a reduction in roughness of AlN buffer layer could lead to improved mobility resulting in enhanced

transport properties [29]. However, further increment in buffer growth temperature to 800 °C resulted in morphological transition in AlGaIn film from highly smooth surface to a comparatively rough surface as shown in Fig. 5h. The surface is pertaining large amount of nano-sized islands agglomerated and the surface roughness is found to be increased nearly 3 times having $R_{r.m.s.}$ value of 18.2 nm. The surface degradation could be associated to a limited incorporation probability of Al in AlN due to higher substrate temperature and thus lead toward a comparatively degraded quality of AlN buffer layer. This belong to a rise in excess active N on the surface of the film due to increased surface diffusion barrier, that resulted in N-rich growth of buffer layer leading to degraded morphology of AlGaIn epitaxial layer grown on it. Further, the depth profile observed for each AlGaIn film revealed smoothest surface in AlGaIn grown in S-780 (Fig. 5f) among all the samples grown via PAMBE under different buffer growth conditions.

3.3 Optical properties

The influence of buffer layer parameters on optical properties has been explored which will indirectly play a prominent role in deciding the behavior of optoelectronic devices to be developed using AlGaIn [3, 30]. Figure 6a represents the RT-PL spectra of each sample where a sharp NBE emission is observed for every AlGaIn film with a trivial shift in its NBE position leading to slight variation in the

Fig. 6 **a** The RT-PL spectra acquired from the AlGaIn films grown in S-760, S-780 and S-800 samples; **b** the plot showing variation in Al composition with changing buffer condition in each sample; **c** the trends of PL NBE bandwidth and ratio of DB to NBE intensity variation (I_{DB}/I_{NBE}) against each sample grown with different buffer parameters; **d** The micro-Raman Spectra enlarged for the range of 550–750 cm^{-1} ; inset shows the complete Raman spectra in the range of 450–800 cm^{-1}



bandgap of the grown ternary AlGa_xN alloys. The NBE peaks are centered at 312, 309 and 307 nm with error of ± 0.5 nm for samples S-760, S-780 and S-800, respectively.

Further, a shoulder peak to NBE emission was prominently observed at around 327 nm in S-760 (Fig. a) which is ascribed to transitions from shallow donor to shallow acceptor states known as Donor Acceptor Pair (DAP) transitions in the grown AlGa_xN films. This characteristic can be attributed to an exciton bound to a native defect related shallow acceptor states such as any vacancy-related complex [31]. Though, a more prominent DAP could also exist in NBE peak's envelope of other AlGa_xN films in S-780 and S-800 which resulted in broadening of the NBE emission band. This enhanced DAP emission could be attributed to either increased III-group vacancies or influenced by the unintentional doping from the substrate during the growth into the nitride layer [32, 33]. Besides, a broad emission band centered at around 481, 498 and 511 nm in samples S-760, S-780 and S-800, respectively is clearly noticed which is related to the defect states within the energy bandgap of the grown AlGa_xN films [34]. It can be clearly observed that the defect band is significantly suppressed for the film grown in S-780 sample. Next, the bandgap obtained from the NBE emission has been used for evaluating the Al composition (x) by using Vegard's law, [35]

$$E_g^{AlGaN} = x.E_g^{AlN} + (1-x)E_g^{GaN} + b.x.(1-x) \quad (2)$$

where x is the Al mole fraction and b is the bowing parameter, $b = 1.3$ in alloy Al_xGa_{1-x}N [36]. The evaluated composition values are plotted against the sample in Fig. 6b and exhibited an incrementing trend with increasing buffer growth temperature. This suggests that buffer temperature and crystalline quality may lead to slight changes in the bandgap of the material. The Al composition is 30, 31.5 and 33% for S-760, S-780 and S-800, respectively. It was reported that the growth rate significantly affects the Al incorporation efficiency in AlGa_xN growth [37, 38]. Thus, the increased Al incorporation from S-760 to S-800 samples could be related to different growth rates of AlGa_xN with varied AlN buffer growth quality. Although, these values are found to be slightly different from the HRXRD results that could be due to strain present in the grown films which have lead towards this deviation in the HRXRD results. Furthermore, it is known that the FWHM of NBE emission band (Fig. 6c) determines the quality of grown epitaxial film, thus, the changes in buffer growth temperatures resulted in varying the quality of grown AlGa_xN films with least FWHM for sample S-760, which is found to be increased with increasing buffer growth temperature. This could be correlated to the enhanced DAP band existing

along with NBE in complete peak envelope of S-780 and S-800.

On the other hand, Fig. 6c shows the change in ratio of defect band and NBE band extracted from the obtained experimental PL results of each sample. It was observed that the I_{DB}/I_{NBE} value is least for the sample S-780 which signifies high quality AlGa_xN growth with least amount of trap/defect states in the energy bandgap. Therefore, although the FWHM is slightly higher for AlGa_xN film grown in S-780 still, the intensity ratio of defect band to NBE is prominently reduced compared to other two growths carried out in S-760 and S-800. Conclusively, the PL analysis recommend that the optical properties of AlGa_xN film grown in S-780 is superlative compared to the other grown samples and thus, it is highly expected to yield better device efficiency. The optical properties are further analyzed by performing micro-Raman spectroscopy. The Raman measurements have been used to evaluate the energies of phonon modes present in Al_xGa_{1-x}N ternary alloy. Inset of Fig. 6d shows the micro-Raman spectra obtained for a whole range of 450–800 cm^{-1} which yielded a highly dominant Si substrate peak at around 521.5 cm^{-1} in all the AlGa_xN/AlN/Si heterostructures. A closer examination unveils the existence of two modes each one of GaN-like and AlN-like mode branches from the PAMBE grown samples S-760, S-780 and S-800. This implicates two-mode behavior for $E_2(\text{high})$ mode of AlGa_xN [39]. For deeper investigation, the experimental data acquired from the Raman spectra is enlarged from 550–750 cm^{-1} as shown in Fig. 6d. It was perceived that apart from sample S-760, the AlGa_xN grown in other two samples i.e. S-780 and S-800 almost coincides at same GaN-like and AlN-like $E_2(\text{high})$ mode which suggests nearly same Al composition in AlGa_xN grown in samples S-780 and S-800 compared to S-760. The two mode behavior could be responsible for variation in the composition evaluation from HRXRD and the Raman phonon frequencies.

In summary, AlGa_xN film with high crystalline epitaxial quality has been grown by optimizing different AlN buffer layer growth conditions on Si (111) substrate using PAMBE. The AlN buffer has been grown under varied growth temperatures (760 °C to 800 °C) wherein, a highly single crystalline AlGa_xN film with comparatively lowest XRC FWHM value of 2196 arcsec was witnessed when AlN buffer was grown at 780 °C. The quality of AlN buffer layer is found to impact the growth properties as well as the Al incorporation in the grown AlGa_xN films. The morphological analysis reveals highly smooth surface morphology with least surface defect states. Then, the optical properties were analyzed to gauge the influence of buffer layer on the AlGa_xN films where, the RT-PL analysis of sample S-780 revealed a bandgap value of 309 nm resulting in 31.5% Al composition evaluated using the Vegard's law. Along with this,

the defect band to NBE band ratio (I_{DB}/I_{NBE}) is significantly reduced from 0.57 to 0.3 when buffer growth temperature increased from 760 to 780 °C. While, the I_{DB}/I_{NBE} ratio again increased to 0.72 when the buffer temperature increases to 800 °C. Therefore, the structural, morphological and optical properties divulges that the AlGaIn film grown in sample S-780 (where buffer growth temperature is 780 °C) is highly crystalline in nature with minimum defects states. Conclusively, this study determines that the buffer layer temperature plays significant role in controlling the structural and optical properties of AlGaIn layer grown over it.

Acknowledgement We gratefully acknowledge Director, CSIR-NPL, New Delhi, for his encouragement and support. Neha would like to acknowledge CSIR for providing financial assistance via CSIR-Research Associateship.

Compliance with ethical standards

Conflict of interest The authors declare no financial interest.

Open Access This article is licensed under a Creative Commons Attribution 4.0 International License, which permits use, sharing, adaptation, distribution and reproduction in any medium or format, as long as you give appropriate credit to the original author(s) and the source, provide a link to the Creative Commons licence, and indicate if changes were made. The images or other third party material in this article are included in the article's Creative Commons licence, unless indicated otherwise in a credit line to the material. If material is not included in the article's Creative Commons licence and your intended use is not permitted by statutory regulation or exceeds the permitted use, you will need to obtain permission directly from the copyright holder. To view a copy of this licence, visit <http://creativecommons.org/licenses/by/4.0/>.

References

1. Upadhyay KT, Chattopadhyay MK (2021) Sensor applications based on AlGaIn/GaN heterostructures. *Mater Sci Eng, B* 263:114849
2. Dimkou I, Harikumar A, Ajay A, Donatini F, Bellet-Amalric E, Grenier A, den Hertog MI, Purcell ST, Monroy E (2020) Design of AlGaIn/AlN Dot-in-a-Wire Heterostructures for Electron-Pumped UV Emitters. *Physica status solidi (a)* 217(7):1900714
3. Lingaparthi R, Dharmarasu N, Radhakrishnan K, Agrawal M (2020) In-situ stress evolution and its correlation with structural characteristics of GaN buffer grown on Si substrate using AlGaIn/AlN/GaN stress mitigation layers for high electron mobility transistor applications. *Thin Solid Films* 708:138128
4. Alaie Z, Mohammad Nejad S, Yousefi MH (2015) Recent advances in ultraviolet photodetectors. *Mater Sci Semicond Process* 29:16–55
5. Liu L, Edgar JH (2002) Substrates for gallium nitride epitaxy. *Mater Sci Eng: R: Reports* 37:61–127
6. Vittoz S, Rufer L, Rehder G, Heinle U, Benkart P (2010) Analytical and numerical modeling of AlGaIn/GaN/AlN heterostructure based cantilevers for mechanical sensing in harsh environments. *Procedia Eng* 5:91–94
7. Carey P, Ren F, Bae J, Kim J, Pearton S (2020) Wide Bandgap Semiconductor-Based Electronics. IOP Publishing, Bristol
8. Aldalbahi A, Li E, Rivera M, Velazquez R, Altalhi T, Peng X, Feng PX (2016) A new approach for fabrications of SiC based photodetectors. *Scientific Reports* 6:23457
9. Jmerik V, Nechaev D, Rouvimov S, Ratnikov V, Kop'ev P, Rzheutski M, Lutsenko E, Yablonskii G, Aljohenii M, Aljerwii A, Alyamani A, Ivanov S (2015) Structural and optical properties of PA MBE AlGaIn quantum well heterostructures grown on c-Al₂O₃ by using flux- and temperature-modulated techniques. *J Mater Res* 30:2871–2880
10. Koblmuller G, Chu RM, Raman A, Mishra UK, Speck JS (2010) High-temperature molecular beam epitaxial growth of AlGaIn/GaN on GaN templates with reduced interface impurity levels. *J Appl Phys* 107:043527
11. Shim KH, Myoung JM, Gluschenkov OV, Kim C, Kim K, Yoo MC, Kim S, Turnbull DA, Bishop SG (2011) Growth and Characterization of AlGaIn/GaN Heterostructures with Multiple Quantum Wells by PAMBE. *MRS Proceedings* 423:347
12. Ganguly S, Verma J, Xing H, Jena D (2014) Plasma MBE growth conditions of AlGaIn/GaN high-electron-mobility transistors on silicon and their device characteristics with epitaxially regrown ohmic contacts. *Appl Phys Express* 7:105501
13. Pramanik P, Sen S, Singha C, Roy AS, Das A, Sen S, Bhattacharyya A (2016) Compositional inhomogeneities in AlGaIn thin films grown by molecular beam epitaxy: Effect on MSM UV photodetectors. *J Appl Phys* 120:144502
14. Pau JL, Monroy E, Munoz E, Naranjo FB, Calle F, Sanchez-Garcia MA, Calleja E (2001) AlGaIn photodetectors grown on Si(111) by molecular beam epitaxy. *J Cryst Growth* 230:544–548
15. Ristic J, Sanchez-Garcia MA, Calleja E, Sanchez-Paramo J, Calleja JM, Jahn U, Ploog KH (2002) AlGaIn Nanocolumns Grown by Molecular Beam Epitaxy: Optical and Structural Characterization. *Physica status solidi (a)* 192:60–66
16. Liaw HM, Venugopal R, Wan J, Melloch MR (2001) Influence of the AlN buffer layer growth on AlGaIn/GaN films deposited on (111)Si substrates. *Solid-State Electronics* 45:417–421
17. Iliopoulos E, Moustakas TD (2002) Growth kinetics of AlGaIn films by plasma-assisted molecular-beam epitaxy. *Appl Phys Lett* 81:295–297
18. Rudziński M, Zlotnik S, Wójcik M, Gaca J, Janicki Ł, Kudrawiec R (2021) Mask-free three-dimensional epitaxial growth of III-nitrides. *J Mater Sci* 56(1):558–569
19. Mazumder B, Kaun SW, Lu J, Keller S, Mishra UK, Speck JS (2013) Atom probe analysis of AlN interlayers in AlGaIn/AlN/GaN heterostructures. *Appl Phys Lett* 102:111603
20. Aggarwal N, Krishna S, Kumar Jain S, Mishra M, Maurya KK, Singh S, Kaur M, Gupta G (2019) Microstructural evolution of high quality AlN grown by PAMBE under different growth conditions. *Mater Sci Eng: B* 243:71–77
21. Pandey A, Dutta S, Prakash R, Raman R, Kapoor AK, Kaur D (2018) Growth and Comparison of Residual Stress of AlN Films on Silicon (100), (110) and (111) Substrates. *J Electron Mater* 47:1405–1413
22. Norris DA, Rodriguez MA, Fukuda SK, Snyder RL (2013) X-Ray Powder Data for alpha-Si₃N₄. *Powder Diffraction* 5:225–226
23. Ozen S, Senay V, Pat S, Korkmaz S (2015) Investigation on the morphology and surface free energy of the AlGaIn thin film. *J Alloy Compd* 653:162–167
24. Aggarwal N, Krishna S, Goswami L, Gupta G (2021) Inclination of screw dislocations on the performance of homoepitaxial GaN based UV photodetectors. *Mater Sci Eng, B* 263:114879
25. Z. Yang, C. Bingzhen, P. Na, Z. Lu, Y. Cuibai, P. Xu, Y. Shun, W. Zhiyong, Growth of AlGaIn Film on Si (111) Substrate, in: MATEC Web of Conferences, Shanghai, China, 2016.
26. Moram MA, Vickers ME (2009) X-ray diffraction of III-nitrides. *Rep Prog Phys* 72:036502

27. Aggarwal N, Krishna S, Goswami L, Mishra M, Gupta G, Maurya KK, Singh S, Dilawar N, Kaur M (2015) Extenuation of Stress and Defects in GaN Films Grown on a Metal-Organic Chemical Vapor Deposition-GaN/c-Sapphire Substrate by Plasma-Assisted Molecular Beam Epitaxy. *Cryst Growth Des* 15:2144
28. Tetzner H, Sana P, Klesse WM, Capellini G, Schubert MA, Thapa SB, Storck P, Schroeder T, Zoellner MH (2020) Carbon related hillock formation and its impact on the optoelectronic properties of GaN/AlGaIn heterostructures grown on Si(111). *Appl Phys Lett* 116:252101
29. Singh VK, Pandey A, Tyagi R (2020) Optimization of AlN spacer layer in MOVPE grown AlGaIn/AlN/InGaIn/GaN high electron mobility heterostructure. *AIP Conf Proc* 2220:090026
30. Rathkanthiwar S, Kalra A, Remesh N, Bardhan A, Muralidharan R, Nath DN, Raghavan S (2020) Impact of pits formed in the AlN nucleation layer on buffer leakage in GaN/AlGaIn high electron mobility transistor structures on Si (111). *J Appl Phys* 127:215705
31. Reshchikov MA, Morkoç H (2005) Luminescence properties of defects in GaN. *J Appl Phys* 97:061301
32. Paskova T, Arnaudov B, Paskov PP, Goldys EM, Hautakangas S, Saarinen K, Södervall U, Monemar B (2005) Donor-acceptor pair emission enhancement in mass-transport-grown GaN. *J Appl Phys* 98:033508
33. Le LC, Zhao DG, Jiang DS, Wu LL, Li L, Chen P, Liu ZS, Zhu JJ, Wang H, Zhang SM, Yang H (2012) Effect of light Si-doping on the near-band-edge emissions in high quality GaN. *J Appl Phys* 112:053104
34. Krishna S, Aggarwal N, Gundimeda A, Sharma A, Husale S, Maurya KK, Gupta G (2019) Correlation of donor-acceptor pair emission on the performance of GaN-based UV photodetector. *Mater Sci Semicond Process* 98:59–64
35. Vurgaftman I, Meyer JR (2003) Band parameters for nitrogen-containing semiconductors. *J Appl Phys* 94:3675–3696
36. Angerer H, Brunner D, Freudenberger F, Ambacher O, Stutzmann M, Hopler R, Metzger T, Born E, Dollinger G, Bergmaier A, Karsch S, Korner HJ (1997) Determination of the Al mole fraction and the band gap bowing of epitaxial Al_xGa_{1-x}N films. *Appl Phys Lett* 71:1504–1506
37. Deng Y, Zhao DG, Le LC, Jiang DS, Wu LL, Zhu JJ, Wang H, Liu ZS, Zhang SM, Yang H, Liang JW (2011) Relationship between the growth rate and Al incorporation of AlGaIn by metalorganic chemical vapor deposition. *J Alloy Compd* 509:748–750
38. Li D-B, Aoki M, Katsuno T, Miyake H, Hiramatsu K, Shibata T (2007) Influence of growth conditions on Al incorporation to Al_xGa_{1-x}N (x>0.4) grown by MOVPE. *J Cryst Growth* 298:372–374
39. Harima H (2002) Properties of GaN and related compounds studied by means of Raman scattering. *J Phys: Condens Matter* 14:R967–R993

Publisher's Note Springer Nature remains neutral with regard to jurisdictional claims in published maps and institutional affiliations.